PERGAMON

International Journal of Heat and Mass Transfer 45 (2002) 4773–4780

International Journal of HEAT and MASS TRANSFER

www.elsevier.com/locate/ijhmt

Optimization of the design factors for thermal performance of a parallel-flow heat exchanger

Kilyoan Chung, Kwan-Soo Lee *, Woo-Seung Kim

School of Mechanical Engineering, Hanyang University, 17 Haengdang-dong, Sungdong-gu, Seoul 133-791, South Korea

Received 28 September 2001; received in revised form 10 May 2002

Abstract

The heat and flow analyses of a parallel-flow heat exchanger are performed. Two models with and without considering the effects of the geometric characteristic of flat tube are used. Comparing the two models, the modeling using the heat transfer correlations of flat tubes shows the better accuracy and stability of numerical solutions. The effect of flow distribution on the thermal performance is examined with varying the design factors (i.e., the locations of separators and inlet/outlet, and the aspect ratios of microchannels of the heat exchanger). The flow uniformities along the paths of the heat exchanger are proposed, and are observed to evaluate the thermal performance of the heat exchanger. The optimization using the ALM method has been accomplished by maximizing the flow uniformity. It is found that the heat transfer rate of the optimized model is increased by 6.0% compared to that of the base type and the pressure drop by 0.4%.

1. Introduction

The heat exchangers for refrigeration and air-conditioning systems are often required to be compact in size and light in weight because they are usually installed in confined spaces. The heat capacity of a parallel-flow heat exchanger (PFHE) is 150–200% larger than that of the conventional heat exchanger. The high heat capacity of the PFHE can meet the requirements of compactness and lightness. The PFHE has a good thermal performance, but it is different in structure compared with conventional heat exchangers. Therefore, the study on the internal heat and flow characteristics is required.

Considering the internal shape of the PFHE, it can be modeled as the multiple passages problem. The uniform flow distribution is the most important phenomenon when the heat and flow characteristics of multiple passages problems are considered. Nakamura et al. [1] designed passages of a power transformer using the multi-block method so that the flow distribution of the air in each passage can be uniform. Karvounis and Assanis [2] examined the flow distribution inside a catalytic converter by varying the size of its inlet, based on the fact that the more uniform the distribution of inlet velocity, the more uniform the flow rate in each passage. Choi et al. [3] studied the effects of the inlet size of a cooling fan and the spacing between PCB boards on the uniformity of the flow distribution, with no increase in pumping power, for electronic packaging applications. But it is expected that there will be differences between the multiple passages and PFHE in the heat and flow characteristics because the PFHE is composed of multiple passages with multi-directional flow. In regard to the thermal performance of a PFHE, Sugihara and Lukas [4] explained the basic structure and materials of a PFHE for automobiles, and reported some experimental results on its thermal performance. It has difficulties examining the heat and flow characteristics with varying geometric parameters, because the results of reference [4] are focused on a comparison with the other types of heat exchangers.

In this study, the numerical analysis on the thermal performance of a PFHE is performed. To evaluate the thermal performance, flow uniformity is defined. The design parameters are selected and the effects of these

* Corresponding author. Tel.: +82-2-2290-0426; fax: +82-2-2295-9021.

E-mail address: ksleehy@hanyang.ac.kr (K.-S. Lee).

0017-9310/02/$ - see front matter
PII: S0017-9310(02)00195-3

Nomenclature

A_{in}	diameter of inlet, reference length
A_{out}	diameter of outlet
B	width of header (non-dimension)
C_1, C_2, C_μ	turbulent constants
D	hydraulic diameter
f	friction factor
g_j	constraints
g	gravity (m/s^2)
G	mass flux (kg/m^2 s)
h	convective heat transfer coefficients (W/m^2 K)
h_m	height of microchannel (mm)
$\mathscr{H}$	height of heat exchanger (non-dimension)
k	thermal conductivity (J/kg K)
$\mathscr{L}$	length (non-dimension)
L	length from upper side or lower side (non-dimension)
L_h	louver thickness (non-dimension)
$\dot{m}$	flow rate (kg/s)
NP	number of passages
NPP	number of passages of path
Nu	Nusselt number
P	pressure, $P = 2p/\rho u_{in}^2$
Re_{psg}	Reynolds number, $Re_{psg} = 2Gh_m/\mu$
T	temperature (K)
u, v	dimensionless velocity
U	flow uniformity
W_L	length of louvered fin (non-dimension)

Greek symbols

α	aspect ratio of microchannel
ΔX	length between wall grid point and near grid point
ε	turbulent dissipation rate
η_f	efficiency of louvered fin
θ	non-dimensional temperature, $\theta = (T - T_{air})/(T_{in} - T_{air})$
θ_L	louver angle
κ	turbulent kinetic energy
μ	viscosity (kg/ms)
v	dynamic viscosity (m^2/s)
ρ	density (kg/m^3)
σ_t	turbulent Prandtl number

Subscripts

0	smooth tube ($\alpha = 15$)
e	end or equivalent
eff	effective
f	fin
i, j	tensor indexes
ideal	ideal case
in	inlet
out	outlet
overall	overall
pth	path
psg	passage
t	flat tube

parameters on heat and flow characteristics are examined. To suggest the optimum geometries for the PFHE, the optimum process is applied.

2. Mathematical modeling

A PFHE is composed of headers combining or separating working fluid, flat tubes that are the passages for the working fluid, and separators that determine the path of the passages. Air flows through the frontal area of a PFHE as shown in Fig. 1(a) and the louvered fin (see Table 1) is equipped between the flat tubes to improve the thermal performance. The PFHE (see Fig. 1(a) and Table 1) is chosen as a base type that is commercially available. In the PFHE shown in Fig. 1(a), the heat transfer area of flat tubes occupies most of the overall heat transfer area of the PFHE. The flat tube has several microchannels inside it. Microchannels inside flat tube improve the thermal performance of a PFHE. In this study, the heat and flow analyses are performed using two models on flat tube to investigate the effect of the geometric characteristics of flat tubes on the thermal performance of a PFHE. Two-dimensional plain modeling called "P-modeling" that neglected the effect of microchannels inside flat tube and modeling using the heat transfer correlations of flat tube called "C-modeling". In P-modeling, the physical quantities of the whole passage are numerically computed at each node point. In C-modeling, the whole passage is divided by three parts as shown in Fig. 1(b), and the physical quantities are calculated in a similar fashion as in Section 2.3.

2.1. Governing equation

For the analysis of PFHE, the internal flow is assumed to be two-dimensional, steady, and incompressible turbulent flow. It is also assumed that viscosity and density of the working fluid are kept constant. Phase change is not considered because of the absence of a suitable two-phase model that can be applied to the flat tubes with a small hydraulic diameter. Under these assumptions, the general governing equations in tensor form is as follows:

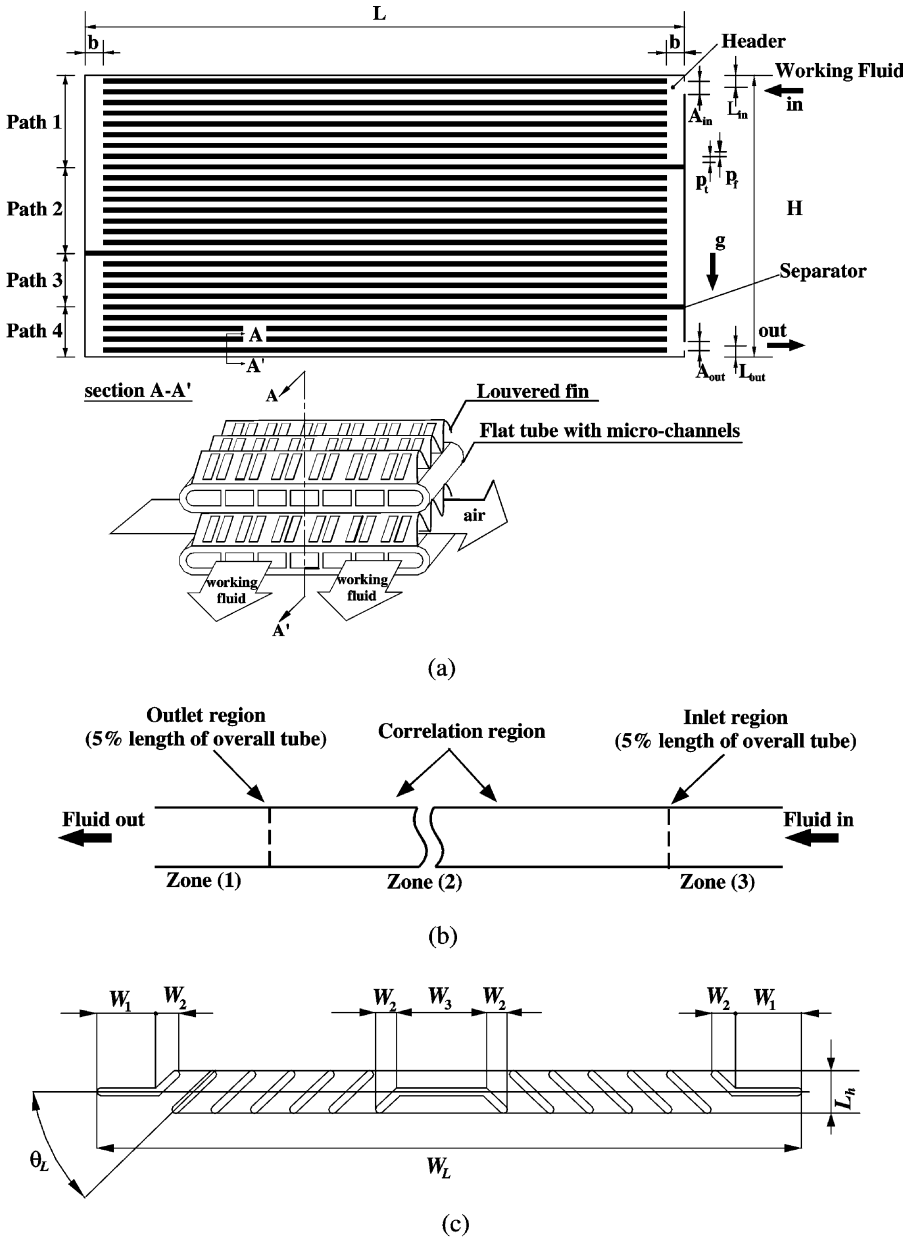

Fig. 1. Physical model of a PFHE: (a) schematic diagram, (b) passage (flat tube) of PFHE, (c) geometry of louvered fin.

Table 1
The geometric specifications of a PFHE (dimensionless)

A_{in}	A_{out}	L_{in}	L_{out}	b
1.00	0.75	1.02	0.87	1.46
$\mathscr{H}$	$\mathscr{L}$	p_f	p_t	θ_L
22.68	48.03	0.71	0.16	24°
W_L	W_1	W_2	W_3	L_h
1.26	0.11	0.04	0.04	0.04

$$\frac{\partial}{\partial x_i}(\rho u_i \hat{q}) = \frac{\partial}{\partial x_i}\left(\mu_{\text{eff}} \frac{\partial \hat{q}}{\partial x_i}\right) + S_{\hat{q}} \tag{1}$$

where $\hat{q}$ becomes 1, u, v, h, κ, or ε for mass, momentum, energy, and turbulent transport equations, respectively. The standard κ–ε model is used for turbulent flow analysis. The source term ($S_{\hat{q}}$) for each variable in equation (1) is listed in Table 2.

Table 2
$\hat{q}$, $\sigma_{\hat{q}}$, and $S_{\hat{q}}$ for governing equation (1)

Equations	$\hat{q}$	$\sigma_{\hat{q}}$	$S_{\hat{q}}$
Continuity	1	–	0
x-momentum	u	1.0	$-\frac{\partial p}{\partial x}+\frac{\partial}{\partial x_i}\left[\mu_{\text{eff}}\left(\frac{\partial u_i}{\partial x}\right)\right]$
y-momentum	v	1.0	$-\frac{\partial p}{\partial y}+\frac{\partial}{\partial x_i}\left[\mu_{\text{eff}}\left(\frac{\partial u_i}{\partial y}\right)\right]-\rho g$
Energy	H	0.9	$\frac{\partial}{\partial x_i}\left[\mu_{\text{eff}}\left(\frac{\partial \Delta H}{\partial x_i}\right)\right]$
k-equation	κ	1.0	$\rho(P_{\text{r}}-\varepsilon)$
ε-equation	ε	1.3	$\rho(\varepsilon/\kappa)(C_1P_{\text{r}}-C_2\varepsilon)$

$\mu_{\text{eff}}=(\mu+\mu_{\text{t}})/\sigma_{\hat{q}}$, $\mu_{\text{t}}=\rho C_\mu\kappa^2/\varepsilon$, $C_1=1.44$, $C_2=1.92$, $C_\mu=0.09$, $P_{\text{r}}=\frac{\mu_{\text{t}}}{\rho}\left[2\left(u_x^2+v_y^2\right)+\left(v_x+u_y\right)^2-\frac{2}{3}\left(u_x+v_y\right)^2\right]$

2.2. Boundary conditions

Boundary conditions of the dimensionless velocity and the dimensionless temperature are as follows:

Dimensionless velocity:

$$\begin{aligned} &u=u_{\text{in}},\ v=0 \quad \text{at the inlet}\\ &u=v=0 \quad \text{at the header and the passage walls}\\ &\int_{\text{in}} u\,\mathrm{dA}=\int_{\text{out}} u\,\mathrm{dA} \quad \text{at the outlet} \end{aligned} \tag{2}$$

Dimensionless temperature:

$$\theta=\theta_{\text{in}}=1 \quad \text{at the inlet}$$

$$\theta_{\text{wall}}=\frac{\theta_{\text{nb}}}{Nu_{\text{out}}\Delta X+1}$$

at the header and the passage walls

$$\frac{\partial\theta}{\partial n}=0 \quad \text{at the outlet} \tag{3}$$

In Eqs. (2) and (3), subscripts 'in, wall, nb, and out' denote inlet, wall, grid next to wall, and outlet, respectively. Nu_{out} in Eq. (3) is the outside Nusselt number at the wall or between the blocks, is defined as

$$Nu_{\text{out}}=\frac{h_{\text{e}}d}{k} \tag{4}$$

where equivalent heat transfer coefficient (h_{e}) is used for considering the air-side heat transfer, and is defined as follows:

$$h_{\text{e}}=\left(1+\eta_{\text{f}}\frac{A_{\text{f}}}{A_{\text{t}}}\right)h \tag{5}$$

where η_{f}, A_{f}, A_{t} and h represent fin efficiency, area of fin and tube, and heat transfer coefficient, respectively. The air-side heat transfer coefficient (h) is calculated by using the heat transfer relation to a louvered fin [5].

2.3. Treatment of passages

The PFHE shown in Fig. 1(a) has many flat tubes, and the heat transfer area of flat tubes occupies most of the overall heat transfer area. The accuracy of numerical solutions should be affected by considering the effect of microchannels inside the flat tube. Therefore, the physical quantities of passages are calculated by the numerical computing in P-modeling and by the heat transfer correlations [6] together with the numerical computing in C-modeling. Bending flow owing to the connection of flat tube to the headers appears at the inlet and outlet of the passages. The developing region resulting from bending flow is shown in the inlet and outlet of the passages. Each passage is divided into three parts in C-modeling to consider the bending flow. The numerical analyses based on the governing equations must be performed in the developing region (see Fig. 1(b)). The length of the developing region is determined by the profiles of temperature and velocity [7], and it is about 5% of the whole passage. In the fully developed region, the correlations are applied to the correlation region as shown in Fig. 1(b).

$$\frac{f}{f_0}=A_0+A_1\alpha+A_2\alpha^2+\frac{A_3}{\alpha}+\frac{A_4}{\alpha^2} \tag{6}$$

$$\frac{Nu}{Nu_0}=B_0+B_1\alpha+B_2\alpha^2+B_3\alpha^3+B_4\left(\frac{\alpha}{10}\right)^4 \tag{7}$$

where α is the aspect ratio of the microchannel, and the coefficients of equations, A_0–A_4 and B_0–B_4 expressed by the function of Reynolds number, are mentioned in Ref. [6]. The above correlations are valid for the range of $150\leqslant Re_{\text{psg}}\leqslant 460$ and $0.74\leqslant\alpha\leqslant 2.00$, and the coefficients of determination are over 0.99. The Reynolds number at each passage (Re_{psg}) is calculated for the correlations as below.

$$Re_{\text{psg}}=\frac{2Gh_{\text{m}}}{\mu} \tag{8}$$

where G is mass flux, h_m is the height of microchannel of flat tube, and μ is the viscosity of the working fluid. The mass flux (G) is calculated using the ratio of flow distributions of each passage and the flow rate at the inlet.

3. Numerical methods and validation

The governing equation (1) is discretized by using the finite difference method. The convective term of the governing equation is discretized by using a 2nd order central difference scheme and the adaptive damping term. The diffusive term is separated with an orthogonal and a non-orthogonal term. The orthogonal term is treated implicitly and the non-orthogonal term is treated explicitly in the source term. The first-order upwind scheme is used for the energy equation. A non-staggered grid system is adapted. A checkerboard pressure that often occurs in a non-staggered grid system is avoided by adding the 4th order pressure damping term into the pressure correction equation. Since there are several regions that do not require computation in the domain, as shown in Fig. 1(a), a multi-block method was incorporated for saving the computation memory and time.

In this study, the number of mesh lines parallel to the passage is important because the accurate calculation of flow distributions in passages determines the accuracy of numerical solutions. To check the grid independency, four cases of different grids (namely: 5-, 10-, 12- and 15-mesh lines/passage) are tested. The proper grid size without affecting the accuracy of the numerical solutions is 12-mesh lines/passage, in both models. The total grid points are 62,749($= 131 \times 479$) and 24,908($= 52 \times 479$) in P- and C-modeling, respectively. In all cases, the convergent solutions are obtained when the sum of errors is less than 0.1% in flow distribution calculated by the velocities, and the sum of the thermal imbalance at each node is less than 10^{-6} for the temperature.

For the determination of accurate and stable modeling, the ratios of the difference of dimensionless temperature and pressure of P- and C-modeling to the field test [8] are shown in Table 3. The Reynolds number at the inlet is 9766. The numbers of passages in the path (NPP) of base type and S_1 type (see Table 4) are 9-8-5-5 and 11-7-5-4, respectively. And Inlet/outlet positions of two types are the same. As shown in Table 3, in the case of P-modeling, the heat transfer and pressure drop are underestimated by 30% and 40% compared with the field test, respectively. In the case of C-modeling, the heat transfer and pressure drop are underestimated by 11% and 17% compared with the field test, respectively. The deviations of the numerical results are $\pm 4\%$ in P-modeling and $\pm 1\%$ in C-modeling. C-modeling improves the accuracy and stability of the numerical solution because of using the heat transfer correlation of the flat tube which incorporates the most heat transfer area of the PFHE mentioned above. Therefore, the following numerical calculations are applied to C-modeling.

Table 3
Comparison of heat transfer and pressure drop between P- and C-modeling

	P-modeling	C-modeling
Base type		
$\Delta\theta/\Delta\theta_{field,base}$	0.60	0.83
$\Delta P/\Delta P_{field,base}$	0.70	0.89
S_1 type		
$\Delta\theta/\Delta\theta_{field,S1}$	0.67	0.85
$\Delta P/\Delta P_{field,S1}$	0.78	0.90

Table 4
Comparison of uniformities, heat transfer, and pressure drop for the base, S-, I-, and O-types

Type	NPP, L_{in}, L_{out}	$U_{overall}(U_1, U_2, U_3, U_4)$	$\Delta\theta/\Delta\theta_{base}$	$\Delta P/\Delta P_{base}$
Base				
	9-8-5-5, 1.02, 0.87	3.95(2.62, 7.77, 3.79, 4.73)	1.00	1.00
S-types				
S_1	11-7-5-4, 1.02, 0.87	3.91(4.88, 4.13, 3.00, 3.01)	1.02	1.17
S_2	8-7-6-6, 1.02, 0.87	2.38(1.92, 3.77, 3.00, 3.82)	0.97	1.03
S_3	9-8-6-4, 1.02, 0.87	3.62(3.91, 2.30, 2.97, 2.98)	0.98	1.20
I-types				
I_1	9-8-5-5, 0.29, 0.87	2.72(1.86, 2.96, 3.79, 4.73)	0.99	1.02
I_2	9-8-5-5, 1.76, 0.87	2.60(1.80, 3.58, 1.93, 8.87)	1.02	1.05
I_3	9-8-5-5, 2.75, 0.87	2.49(1.54, 2.08, 65.36, 4.68)	0.98	1.03
O-types				
O_1	9-8-5-5, 1.02, 0.33	1.77(1.65, 2.91, 1.73, 1.63)	0.97	1.00
O_2	9-8-5-5, 1.02, 2.19	2.26(6.24, 2.10, 1.12, 2.26)	1.00	1.07

4. Results and discussion

The base type (see Fig. 1(a)) and several other types are numerically analyzed. Design factors are selected so that the total volume of the heat exchanger does not change. The increase of heat transfer rate due to the increase of the total heat transfer area is not desirable in the heat exchanger design. Each path and passage has been numbered in an ascending order from top to bottom. The heat transfers and pressure drops of various types are compared with those of the base type. The flow distributions of passages are examined, and then flow uniformities are calculated. Flow uniformity of path (U_{pth}) and overall flow uniformity (U_{overall}) considering the heat transfer area are defined as

$$U_{\text{pth}} = \left\{ \sqrt{\left\{ \sum_{n=N_s}^{N_e} \left(\frac{\dot{m}_{\text{psg},n} - \dot{m}_{\text{psg,ideal}}}{\dot{m}_{\text{psg,ideal}}} \right)^2 \right\} \Big/ (N_e - N_s)} \right\}^{-1} \Bigg|_{\text{pth}} \tag{9}$$

$$U_{\text{overall}} = \text{NP} \left(\sum_{\text{pth}=1}^{\text{NP}} \frac{A_{\text{pth}}}{A_{\text{tot}} U_{\text{pth}}} \right)^{-1} \tag{10}$$

where N_s and N_e represent 'starting passage number' and 'end passage number' at each passage, respectively. Subscripts psg, pth, and 'ideal' indicate passage number, path number, and ideal case, respectively. A_m, A_{tot}, and NP are the heat transfer area of each path, that of the overall PFHE, and the number of the path, respectively.

The flow uniformity of path (U_{pth}) is used for evaluating the thermal performance of each path, and overall flow uniformity (U_{overall}) is done for comparing among types and evaluating the overall heat exchanger. C-modeling is applied for the governing equations in all cases. S-, I-, O-types modify the location of separators, that of the inlets, and that of the outlet, respectively. The representative results (flow uniformities, the heat transfer and pressure drop ratios of each type to the base type) are shown in Table 4.

4.1. The locations of separators

Flow rates of base type and S_{1-3} modifying the location of separators are shown in Fig. 2. S_1 increases the number of passages in path 1. The numbers of passages are almost uniformly distributed in S_2. S_3 changes the number of passages in paths 3 and 4 compared with the base type. Flow uniformities and the ratios of the heat transfer and pressure drop are shown in Table 4. One noticeable trend is that the flow rates are slightly greater at the lower passages (i.e., larger passage number) than

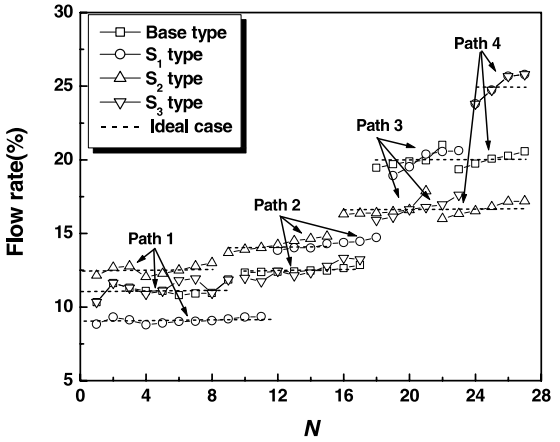

Fig. 2. Flow distribution rates in each passage of the base type and S-types.

at the upper passages (i.e., smaller passage number) for all paths. This may be due to the gravity of the working fluid in all types. Also the pressure drop is larger at the lower passage of each path. In Table 4, overall flow uniformity of S_1 type is decreased by decreasing flow uniformities of paths 2, 3, and 4. But the heat transfer of S_1 is increased by 2% compared with that of the base type because the flow uniformity of path 1, which occupies larger heat transfer area, is increased. The worse thermal performance shown in S_2 type is caused by the decrease of flow uniformities in all paths. S_3 type, similar to the base type, shows the lower values of flow uniformities. The flow uniformity of path 4, which decreases the number of passages in path 4 compared with that of the base type, is largely decreased. The results of the heat transfer and the pressure drop for the various locations of separators indicate that the value of U_1 in S_2 with the number of passages in path 1 less than 9 is decreased significantly and the value of U_4 in S_1 and S_3 types with the number of passages in path 4 less than 5 is also drastically decreased compared to the other cases. Therefore, in the present PFHE with a fixed number of passages of 27, the base type with 9 passages in paths 1 and 5 passages in path 4 shows the best thermal performance.

4.2. The locations of the inlet and the outlet

U_{pth}, U_{overall}, $\Delta\theta/\Delta\theta_{\text{base}}$, and $\Delta P/\Delta P_{\text{base}}$ are listed in Table 4. In the case of I_1 type, the inlet is located toward the upper side of path 1. The flow is relatively concentrated on passage 1 (located in the upper side of path 1). The flow rate of the other passages (except passage 1), affected by the body force, is larger at the lower passages. In the case of I_2 and I_3 types, the inlet is located downward. The flow of the passages above the inlet is

not adequately distributed, and it decreases U_{pth} and $U_{overall}$, simultaneously. Therefore, the location of the inlet is adjusted upward compared with the base type for improving the heat transfer and the pressure drop of the PFHE.

In the case of the O_1 type, the location of the outlet moves to the lowest part of path 4. Flow uniformity of path 4 and overall flow uniformity are decreased because the flow is concentrated on the lowest passage (27) parallel to the outlet. On the contrary, in the case of O_2 type, the location of the outlet moves upward. The working fluid passing through path 4 does not flow out smoothly and some part of the working fluid is stagnated through the lower part of path 4. It highly elevates the pressure drop and degrades the thermal performance of the PFHE. If the outlet is located between passages 26 and 27, the flow uniformity is increased and thus improves the thermal performance. It is shown in Table 4 that the heat transfer and the pressure drop are changed by 1.8% and 2.7%, respectively, according to the location of the inlet. Table 4 also indicates that the heat transfer and the pressure drop are changed by 1.3% and 7.2%, respectively, according to the location of the outlet. The change of the locations of the outlet gives a large influence on the pressure drop.

4.3. Aspect ratio of microchannel

Flat tubes with microchannels are used as the passages of the working fluid in the PFHE. When the width of the tube is fixed, the aspect ratio of the microchannels determines the number of the microchannels. It changes the heat transfer and pressure drop. If the width of the tube is changed, the overall volume of the PFHE is changed. It causes the change of the heat transfer area, and varying the configuration of the louvered fins changes the convective heat transfer coefficient. Thus, the width of the tubes and the configuration of the PFHE are fixed as those of the base type.

Both the heat and flow characteristics of the PFHE are investigated for various aspect ratios of the flat tube. The increase of flow resistance of the microchannels hinders both the effect of the location of the inlet and the concentration of flow rate on the lower passages. The heat transfer and pressure drop ratios are shown in Fig. 3. In Fig. 3, the temperature curve is located above the pressure curve at the range of aspect ratio from 0.8 to 1.3; otherwise the pressure curve is located above the temperature curve. The larger heat transfer appears at the range of aspect ratio from 0.8 to 1.3. In the figure, the slope of the temperature curve is decreased, and that of the pressure curve is increased when the aspect ratio is about 1.0. The large difference between the temperature curve and the pressure curve is shown in the aspect ratio 1.0. Hence, it is expected that best thermal performance occur around the aspect ratio of 1.0. It is also shown that flow uniformity shows a high value in the aspect ratio around 1.0.

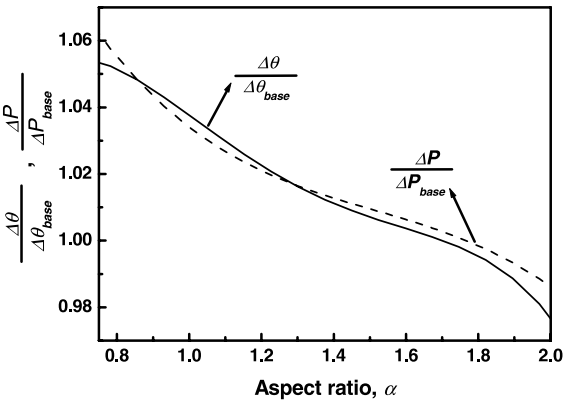

Fig. 3. The ratios of heat transfer and pressure drop with various aspect ratios.

5. Optimization

The effect of the design parameters on the thermal performance is examined. These are the locations of separators and the inlet/outlet, and the aspect ratio of the microchannels. The optimum array of the PFHE is 9-8-5-5, which is the same as that of the base type. The optimum process does not consider the location of separators because it is impossible to express the locations of separator as a continuous function.

The overall flow uniformity ($U_{overall}$) is the evaluation parameter of the PFHE that considers the heat transfer and pressure drop. For performing the optimum process, flow uniformity is approximated as the appropriate polynomial function of L_{in}, L_{out} or α. For approximating, additional numerical results are performed and these are shown in Table 5. The final object function is expressed as the products of normalized flow uniformities as indicated below.

$$\bar{F}(L_{in}, L_{out}, \alpha) = \overline{U}_{overall}(L_{in})\overline{U}_{overall}(L_{out})\overline{U}_{overall}(\alpha) \qquad (11)$$

where $\bar{F}$ and $\overline{U}$ are the approximated functions. Eq. (11) is defined as the following optimum problem under given conditions.

Table 5
Additional values of $U_{overall}$ for I- and O-types

I-types	$U_{overall}$	O-types	$U_{overall}$
$L_{in} = 0.39$	2.90	$L_{out} = 1.34$	3.18
$L_{in} = 1.97$	2.51	$L_{out} = 1.65$	2.64
$L_{in} = 2.36$	2.50	$L_{out} = 0.63$	2.78
		$L_{out} = 0.47$	2.10

$$\text{Min: } F(L_{\text{in}}, L_{\text{out}}, \alpha) = \text{Norm}[\bar{F}(L_{\text{in}}, L_{\text{out}}, \alpha)]^{-1} \tag{12}$$

$$0.825 \leqslant \alpha \leqslant 2.00, \quad 0.294 \leqslant L_{\text{in}} \leqslant 2.746,$$
$$0.332 \leqslant L_{\text{out}} \leqslant 2.189 \tag{13}$$

where Eqs. (12) and (13) are the object function and the constraints, respectively. The ALM method is used for finding the minimum value of the multi-variable problem. For the determination of searching directions, the Broyden–Fletcher–Goldfarb–Shanno method is used. The golden section method is used together with the polynomial approximation [9] for updating the design parameters. The final object function for the ALM method is expressed as below:

$$A(L_{\text{in}}, L_{\text{out}}, \alpha, \lambda, r_{\text{p}}) = F(L_{\text{in}}, L_{\text{out}}, \alpha) + \sum_{j=1}^{3} [\lambda_j \varphi_j + r_{\text{p}} \varphi_j^2]$$

$$\varphi_j = \text{Max}\left[g_j(L_{\text{in}}, L_{\text{out}}, \alpha), -\frac{\lambda_j}{2r_{\text{p}}} \right] \tag{14}$$

where λ is the Lagrangian multiplier, and g_j are the constraints.

The optimum values of the design parameters are $L_{\text{in}} = 0.789$, $L_{\text{out}} = 1.060$, and $\alpha = 1.08$. The approximated value of the overall flow uniformity is 4.65 for these values. This value of the overall flow uniformity for the optimum process is validated for the proposed PFHE. Its flow non-uniformity shows an error of 1.7% compared with the approximated flow uniformity. This means that the approximated functions are valid, and the proposed optimum geometries are well applied when designing the PFHE. Finally $\Delta\theta/\Delta\theta_{\text{base}} = 1.060$, $\Delta P/\Delta P_{\text{base}} = 1.004$, indicate that the heat transfer of the optimum PFHE is increased by approximately 6.0%, and the pressure drop is increased by 0.4%, compared to those of the reference model. The optimum PFHE improves the thermal performance because the increment of heat transfer is much larger than that of the pressure drop.

6. Conclusions

Both the heat and flow analyses of a PFHE, applying two models, are performed. Comparing the two models, the modeling using the heat transfer correlations of the flat tube shows better accuracy and stability of the numerical solutions. For investigating the effect of the flow distribution on the thermal performance, flow uniformities are used. On investigations varying the design factors, 9 and 5 passages are required for paths 1 and 4 such as in the base type for the locations of the separators. The location of the outlet affects the pressure drop. The optimum value of aspect ratio is around 1.0. Finally, the proposed geometrical values obtained by the optimum process are $L_{\text{in}} = 0.789$, $L_{\text{out}} = 1.060$, and $\alpha = 1.08$. The heat transfer and the pressure drop of the optimum PFHE are increased by 6.0% and 0.4%, respectively, compared to those of the base type.

Acknowledgements

The authors would like to thank the Ministry of Science and Technology, Korea, for the financial support by a grant from the Critical Technology 21 Project.

References

[1] Y. Nakamura, W. Jia, M. Yasuhara, Incompressible flow through multiple passages, Numer. Heat Transfer 16 (1989) 451–465.
[2] E. Karvounis, D.N. Assanis, The effect of inlet flow distribution on catalytic conversion efficiency, Int. J. Heat Transfer 36 (6) (1993) 1495–1504.
[3] S.H. Choi, S. Shin, Y.I. Cho, The effect of area ratio on the flow distribution in liquid cooling module manifolds for electronic packaging, Int. Comm. Heat Mass Transfer 20 (1993) 221–234.
[4] A. Sugihara, H.G. Lukas, Performance of parallel flow condensers in vehicular applications, SAE Technical Paper Series 900597 (1990) 1–16.
[5] Y.J. Chang, C.C. Wang, A generalized heat transfer correlation for louvered fin geometry, Int. J. Heat Mass Transfer 40 (3) (1997) 533–544.
[6] K. Chung, K.-S. Lee, W.-S. Kim, Thermal and flow analysis of the flat tube with microchannels, J. KSME (B) 23 (8) (1999) 978–986.
[7] W.M. Kays, M.E. Crawford, Convective heat and mass transfer, International ed., McGraw-Hill, Inc., 1993.
[8] Private communication with Doowon Co. in Korea.
[9] G.N. Vanderplaates, Numerical Optimization Techniques for Engineering Design, International ed., McGraw-Hill, Inc., 1993.